Ebola Virus Sequesters IRF3 in Viral Inclusion Bodies to Evade Host Antiviral Immunity

Lin Zhu[a], Jing Jin[b], Tingting Wang[b], Yong Hu[a], Hainan Liu[a], Ting Gao[a], Qincai Dong[a], Yanwen Jin[a], Ping Li[a], Zijing Liu[a], Xuan Liu[a,*], Cheng Cao[a,*].

Affiliations:

[a]Institute of Biotechnology, Academy of Military Medical Sciences, Beijing, 100850, China

[b]Institute of Physical Science and Information Technology, Anhui University, Hefei, Anhui 230601, China

*Corresponding to:

Cheng Cao (Phone: +86-10-66931932; E-mail: caoc@nic.bmi.ac.cn)

Xuan Liu (Phone: +86-10-66931932; Email: liux931932@163.com)

Running head: EBOV inclusion bodies are involved in immune evasion

Abstract

Viral inclusion bodies (IBs) are commonly formed during the replication of Ebola virus (EBOV) in infected cells, but their role in viral immune evasion has rarely been explored. Here, we found that interferon regulatory factor 3 (IRF3), but not TANK-binding kinase 1 (TBK-1) or IκB kinase epsilon (IKKε), was recruited and sequestered in viral IBs when the cells were infected by EBOV transcription- and replication-competent virus-like particles (trVLPs). NP/VP35-induced IBs formation was critical for IRF3 recruitment and sequestration, probably through STING interaction. Consequently, the association of TBK1 and IRF3, which plays a vital role in type I interferon (IFN-I) induction, was blocked by EBOV trVLPs infection. Additionally, IRF3 phosphorylation and nuclear translocation induced by Sendai virus (SeV) or poly(I:C) stimulation were also suppressed by EBOV trVLPs. Furthermore, downregulation of STING significantly attenuated VP35-promoted IRF3 accumulation in IBs. Viral proteins by which IBs-like structures could be formed were demonstrated to be much more potent in IFN-I antagonism than the expression of the IFN-I antagonist VP35 only. These results suggested a novel immune evasion mechanism by which EBOV evades host innate immunity.

Impact statement: Ebola virus VP35 protein evades host antiviral immunity by interacting with STING to sequester IRF3 into inclusion bodies and inhibit type-I interferon production.

41 **Introduction**

42 Ebola virus disease is the deadliest infectious disease caused by infection with Ebola
43 virus (EBOV), an enveloped, nonsegmented negative-sense RNA virus (Feldmann,
44 Jones, Klenk, & Schnittler, 2003). The 19-kb viral genome comprises seven genes
45 encoding the nucleoprotein (NP), virion protein 35 (VP35), VP40, glycoprotein (GP),
46 VP30, VP24 and RNA-dependent RNA polymerase (L) (Mahanty & Bray, 2004).
47 Inclusion bodies (IBs) formed in EBOV-infected cells are specialized intracellular
48 compartments that serve as sites for EBOV replication and the generation of progeny
49 viral RNPs (Hoenen et al., 2012; Nanbo, Watanabe, Halfmann, & Kawaoka, 2013). In
50 IBs, the EBOV genome is replicated and transcribed by viral polymerase complexes
51 (Misasi & Sullivan, 2014). VP35 serves as a cofactor of RNA-dependent RNA
52 polymerase and contributes to viral replication by homo-oligomerization through a
53 coiled-coil domain (Reid, Cardenas, & Basler, 2005), in addition to its recently
54 discovered presence of phosphorylation and ubiquitination (van Tol et al., 2022; Zhu
55 et al., 2020).

56 Innate interferon responses constitute the first lines of host defense against viral
57 infection. Retinoic acid-inducible gene I (RIG-I)-like receptors, including RIG-I and
58 melanoma differentiation-associated protein 5, play pivotal roles in the response to
59 RNA virus infection. After the recognition of RNA virus infection, RIG-I is recruited
60 to the mitochondrial antiviral adaptor protein (MAVS) through the caspase activation
61 and recruitment domain. The activation of MAVS recruits multiple downstream

signaling components to mitochondria, leading to the activation of inhibitor of κ-B kinase ε (IKKε) and TANK-binding kinase 1 (TBK1), which in turn phosphorylate IFN regulatory factor 3 (IRF3). Phosphorylated IRF3 forms a dimer that translocates to the nucleus, where it activates the transcription of type I interferon (IFN-I) genes (Fitzgerald et al., 2003; Liu et al., 2015).

To promote viral replication and persistence, viruses have evolved various strategies to evade or subvert host antiviral responses. For example, severe fever with thrombocytopenia syndrome virus (SFTSV) has developed a mechanism to evade host immune responses through the interaction between nonstructural proteins and IFN-I induction proteins, including TBK1, IRF3 and IRF7 (Hong et al., 2019; Lee & Shin, 2021; Ning et al., 2014; Wu et al., 2014), sequestering them inside SFTSV-induced cytoplasmic structures known as IBs. In addition to inhibiting IFN-I induction, SFTSV nonstructural proteins can hijack STAT1 and STAT2 in IBs to suppress IFN-I signaling (Ning et al., 2015). These studies highlight the role of viral IBs as virus-built "jails" that sequester some crucial host factors and interfere with the corresponding cellular processes.

EBOV uses various approaches to evade the host immune response, including antagonizing IFN production, inhibiting IFN signaling, and enhancing IFN resistance (Basler et al., 2000; McCarthy et al., 2016; Reid et al., 2006). VP35 is an IFN-I inhibitor that antagonizes host innate immunity by interacting with TBK1 and IKKε (Basler et al., 2003; Prins, Cardenas, & Basler, 2009), suppressing RNA silencing and

83 inhibiting dendritic cell maturation (Haasnoot et al., 2007; Yen, Mulder, Martinez, &
84 Basler, 2014). Here, we report that viral IBs in EBOV trVLPs-infected cells appear to
85 play a role in immune evasion by sequestering IRF3 into IBs and preventing the
86 interaction of IRF3 with TBK1 and IKKε.

87

88 **Results**

89 **IRF3 is hijacked into cytoplasmic IBs in EBOV transcription and**
90 **replication-competent virus-like particles infected cells**

91 When HepG2 cells were infected with EBOV transcription and
92 replication-competent virus-like particles (trVLPs) (Hoenen, Watt, Mora, & Feldmann,
93 2014), which authentically model the complete virus life cycle, IBs with a unique
94 structure and viral particles formed in the cytoplasm (Fig. 1 – figure supplement
95 1A-B). Surprisingly, we found that a substantial percentage of endogenous IRF3 was
96 trapped in viral IBs in EBOV trVLP-infected cells with large IBs (Fig. 1A), while no
97 detectable TBK1 or IKKε, the essential upstream components of IRF3 signaling
98 (Fitzgerald et al., 2003), was sequestered in the viral IBs (Fig. 1B and 1C). These
99 results suggested that IRF3 was specifically compartmentalized in viral IBs, and this
100 compartmentalization spatially isolated IRF3 from its upstream activators TBK1 and
101 IKKε.

Fig. 1

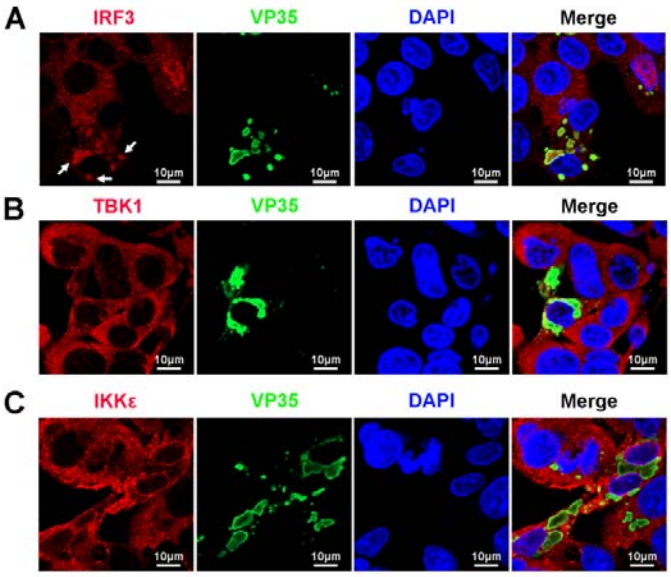

Fig. 1 IRF3, but not TBK1 and IKKε, is sequestered into viral inclusion bodies (IBs) upon EBOV trVLPs infection. (A), HepG2 cells transfected with the EBOV minigenome (p0) were immunostained with anti-IRF3 (red) and anti-VP35 (green) antibodies. White arrows: IRF3 in IBs. (B and C), HepG2 cells transfected with the EBOV minigenome (p0) were immunostained with anti-TBK1 (red in (B)) or anti-IKKε (red in (C)) and anti-VP35 (green in (B and C)) antibodies. Nuclei were stained with DAPI (blue), and images were obtained using a Zeiss LSM 800 Meta confocal microscope. Scale bar, 10 μm.

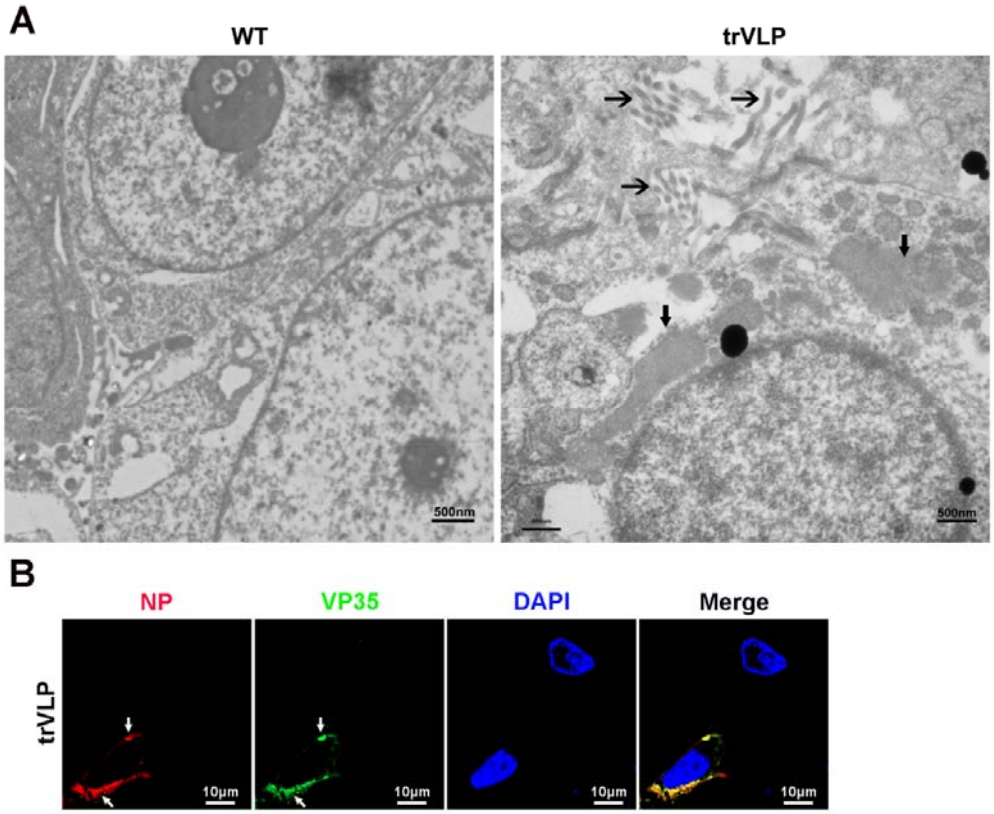

Fig. 1 – figure supplement 1. Transmission electron microscopy and immunofluorescence detection of EBOV trVLPs and IBs. (A), HepG2 cells transfected with or without EBOV trVLP (p0) were fixed and observed with a HITACHI H-7650 transmission electron microscope at an accelerating voltage of 80 kV. The IBs and viral particles (right panel) are marked with bold arrows and regular arrows, respectively. Scale bar, 500 nm. (B), HepG2 cells transfected with the EBOV minigenome (p0) were immunostained with anti-NP (red) and anti-VP35 (green) antibodies. Nuclei were stained with DAPI (blue), and images were obtained using a Zeiss LSM 800 Meta confocal microscope. Scale bar, 10 μm.

IBs sequestration of IRF3 was further investigated at different hours post infection (hpi) of EBOV trVLPs. Detectable IRF3 puncta colocalized with viral

122 proteins were apparent at 36 hpi in infected cells and correlated significantly with the
123 size and shape of the viral IBs (Fig. 2A and 2B). As the size of IBs increased at 48 hpi,
124 nearly all IRF3 colocalized with viral IBs, whereas the IRF3 distribution was
125 completely different in the uninfected cells nearby (Fig. 2A and 2B). Using a
126 fluorophore line of interest analysis, we assessed the intensity profiles of cytoplasmic
127 IRF3 intensity in IBs as well as the increase in the diameter of the aggregates (Fig.
128 2C). As infection proceeded, the intensity of the IRF3 signal in the puncta increased
129 as the level of cytoplasmic-dispersed IRF3 decreased (Fig. 2A), indicating that the
130 total amount of IRF3 in the cells did not dramatically change during infection (Fig.
131 2D) and that only its subcellular localization changed. Taken together, the results
132 above showed that IRF3, but not TBK1 or IKKε, was sequestered in viral IBs.

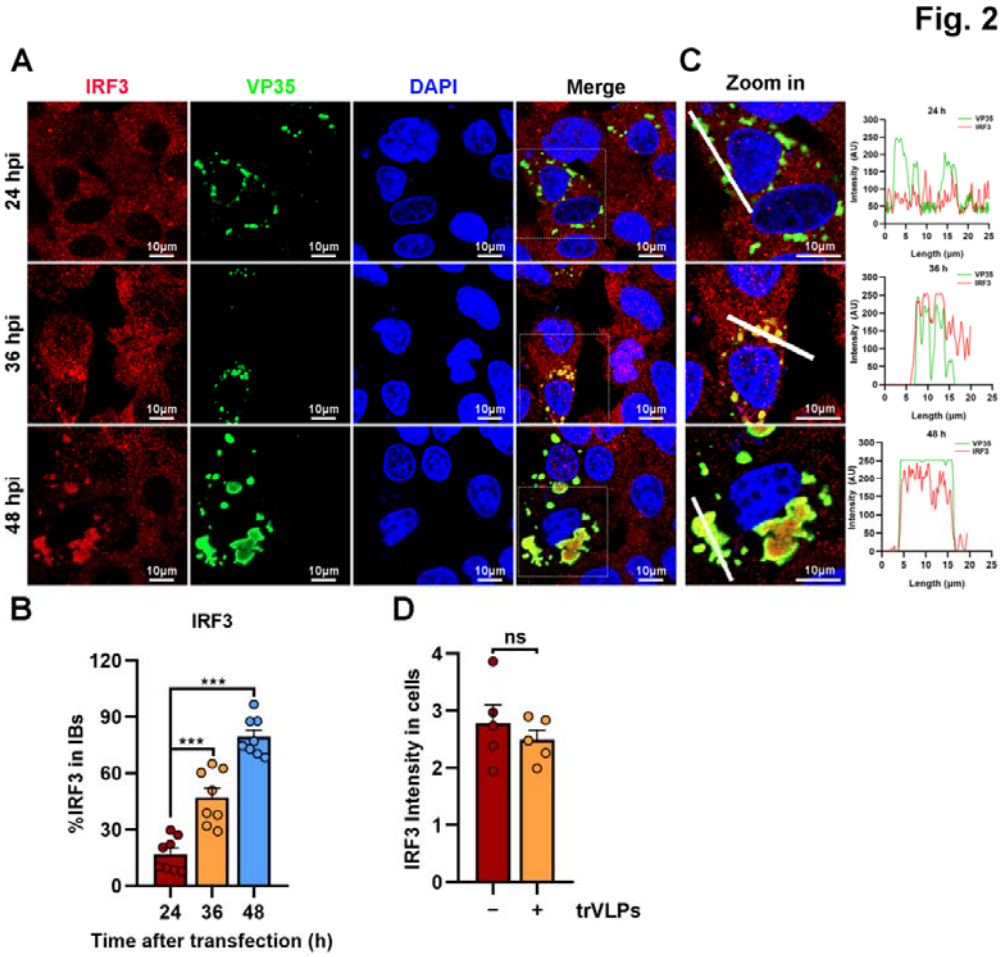

Fig. 2 EBOV trVLP induced the recruitment of IRF3 into intracytoplasmic IBs. (A), HepG2 cells were transfected with the EBOV minigenome (p0). At the indicated time points posttransfection, cells were fixed and immunostained with anti-IRF3 (red) and anti-VP35 (green) antibodies. Nuclei were stained with DAPI (blue), and images were obtained using a Zeiss LSM 800 Meta confocal microscope. Scale bar, 10 μm. The data from two independent replicates are presented. (B), The percentage of IRF3 distribution in IBs at different time points in cells infected with EBOV trVLPs (A) was analyzed with R programming language. The intensity of IRF3 in 8 cells from two independent assays is presented as the mean ± SEM (n=8; ***$P < 0.001$). (C), The left panel shows a magnified image of the IBs boxed in the merged panel of (A). The graphs (right

panel) show fluorescent intensity profiles along the indicated white lines drawn across one or more IBs. (D), The IRF3 intensity in cells infected with or without EBOV trVLPs for 48 h (the lower panel of (A)) was analyzed by ImageJ software. Differences between the two groups were evaluated using a two-sided unpaired Student's *t*-test. The intensity of IRF3 in 5 cells from two independent assays is presented as the mean ± SEM (n=5; ns, not significant).

EBOV trVLPs infection attenuates the TBK1-IRF3 association and IRF3 nuclear translocation

Upon virus infection, IRF3, as a critical transcription factor in the IFN induction pathway, can be phosphorylated and activated by TBK1, and then phosphorylated IRF3 translocates from the cytoplasm into the nucleus, eliciting the expression of antiviral IFNs. Given the sequestration of IRF3 by EBOV trVLPs in IBs, the TBK1-IRF3 association in EBOV trVLPs-infected cells was accessed by an *in situ* Duolink proximity ligation assay (PLA). Cytoplasmic complexes consisting of endogenous TBK1 with IRF3 (the red signal) were observed in HepG2 cells treated with poly(I:C), which induces the activation of the RIG-I signal cascade and IRF3 phosphorylation, and poly(I:C)-induced TBK1: IRF3 complexes were significantly reduced by EBOV trVLPs infection (Fig. 3A and 3B). Decreased TBK1-IRF3 association was further demonstrated by immunoprecipitation (Fig. 3C). Moreover, as shown in Fig. 3D, SeV infection-induced IRF3 phosphorylation and nuclear translocation were significantly inhibited by EBOV trVLPs (Fig. 3D, 4A and 4B).

164 Importantly, IRF3 was also recruited into IBs-like compartments in the cytoplasm in
165 the cells infected with live EBOV (Fig. 4C). These data collectively suggested that the
166 EBOV-mediated sequestration of IRF3 in IBs blocks IRF3 phosphorylation and
167 nuclear translocation in the TBK1-IRF3 signaling cascade, which is critical for IFN
168 induction.

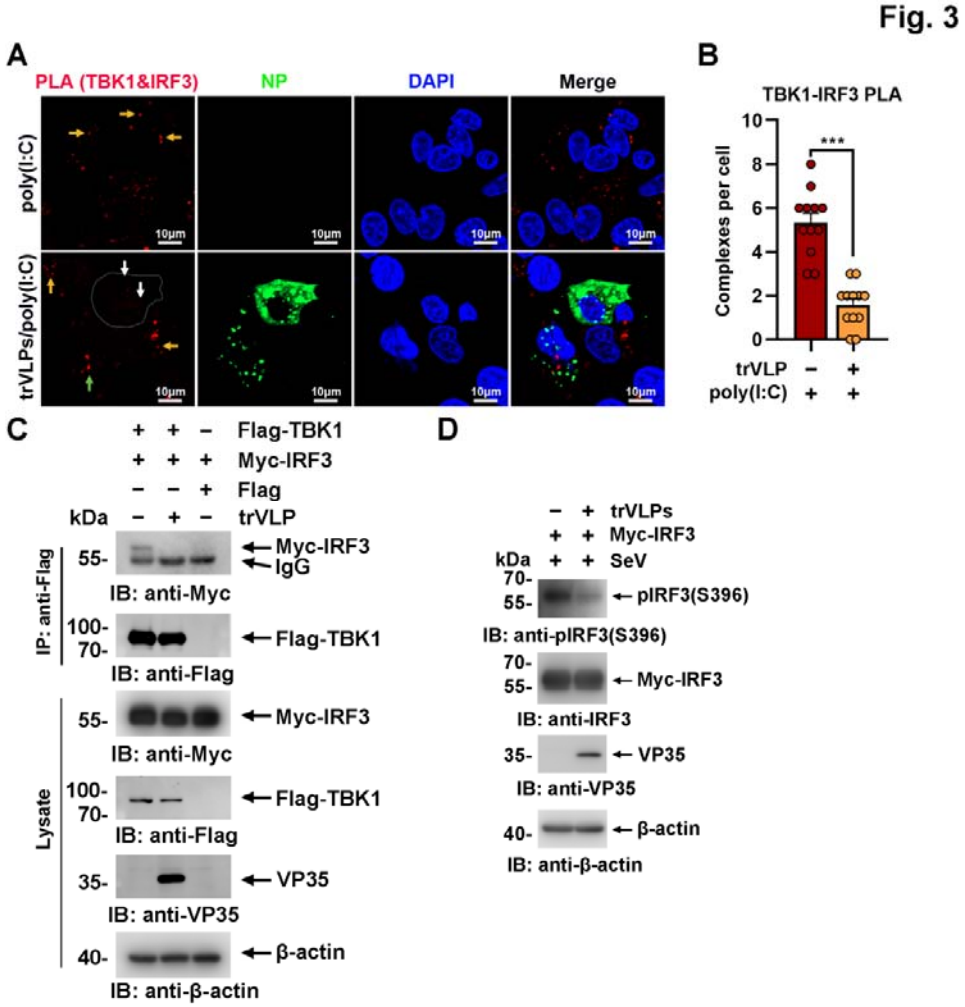

169

170 **Fig. 3 EBOV trVLPs inhibited IRF3 activation.** (A), HepG2 cells were transfected with or
171 without the EBOV minigenome (p0). Thirty-six hours after transfection, the cells were treated
172 with or without 5 μg/ml poly(I:C) for 12 h and then subjected to *in situ* PLA with anti-TBK1 and

173 anti-IRF3 antibodies and immunostaining with an anti-NP antibody (green). Nuclei were stained
174 with DAPI (blue), and images were obtained using a Zeiss LSM 800 Meta confocal microscope.
175 Arrows: white arrows represent TBK1-IRF3 complexes in trVLPs-infected cells, and yellow and
176 green arrows represent TBK1-IRF3 complexes in uninfected and infected cells with small IBs,
177 respectively. Scale bar, 10 μm. (B), The signal for the PLA complex in each cell in (A) was
178 counted from at least 12 cells and is presented as the mean ± SEM. (C), Lysates of HEK293 cells
179 cotransfected with or without the EBOV minigenome (p0) and the indicated plasmids were
180 subjected to anti-Flag immunoprecipitation and analyzed by immunoblotting. (D), HEK293 cells
181 were cotransfected with or without the EBOV minigenome (p0) and Myc-IRF3 plasmids.
182 Thirty-six hours after transfection, the cells were infected with SeV at an MOI of 2 for 12 h, and
183 the phosphorylation of IRF3 was analyzed by immunoblotting with an anti-IRF3-S396 antibody.

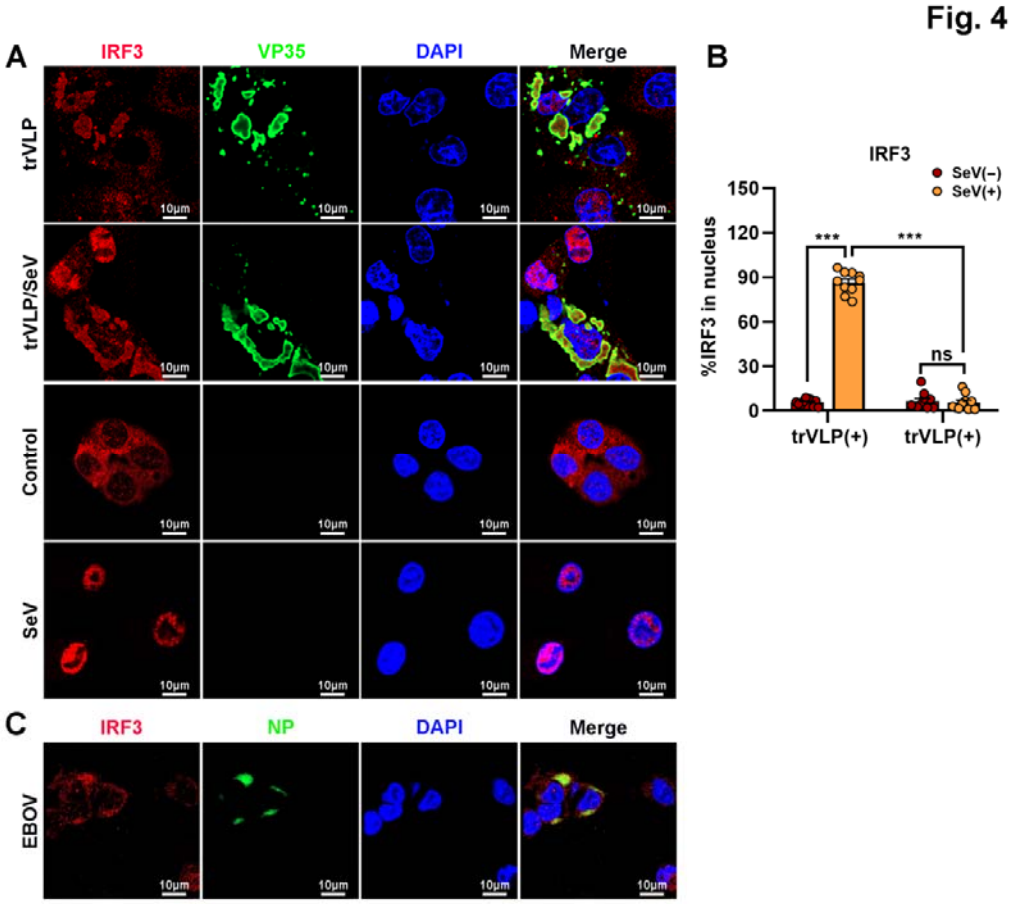

184

185 **Fig. 4 EBOV trVLPs inhibited nuclear translocation of IRF3.** (A), HepG2 cells were
186 cotransfected with or without the EBOV minigenome (p0) for 36 h, and the cells were infected
187 with or without SeV at an MOI of 2 for another 12 h. Then, the cells were fixed and
188 immunostained with anti-IRF3 (red) and anti-VP35 (green) antibodies. Nuclei were stained with
189 DAPI (blue), and images were obtained using a Zeiss LSM 800 Meta confocal microscope. Scale
190 bar, 10 μm. (B), The percentage of IRF3 nuclear distribution in (A) was analyzed by ImageJ
191 software. The ratio of IRF3 distribution in ten cells from two independent assays is presented as
192 the mean ± SEM (ns, not significant, ***$P < 0.001$). (C), HepG2 cells infected with live EBOV
193 (MOI=10) for 72 h were immunostained with anti-IRF3 (red) and anti-NP (green) antibodies.
194 Nuclei were stained with DAPI (blue), and images were obtained using a Zeiss LSM 800 Meta

195 confocal microscope. Scale bar, 10 μm.

196

197 **IBs-like structures formed by the viral proteins VP35 and NP play a key role in**
198 **inducing IRF3 sequestration.**

199 Ectopic expression of NP alone (Noda, Watanabe, Sagara, & Kawaoka, 2007) or
200 NP and the VP35 protein (Noda, Kolesnikova, Becker, & Kawaoka, 2011) in cells
201 was sufficient to form IBs-like structures. To investigate the viral protein(s) involved
202 in the sequestration of IRF3 in IBs, HepG2 cells were transiently transfected with
203 plasmids encoding NP/VP35, NP/VP35/L, NP/VP35/L/VP30,
204 NP/VP35/L/VP30/VP24, or NP/VP35/L/VP30/vRNA-RLuc/T7 and stained with
205 anti-IRF3 and anti-NP at 48 hpi. Coexpression of NP and VP35 resulted in substantial
206 sequestration of IRF3 in the IBs-like structure, which in turn resulted in a significant
207 reduction of IRF3 in the nucleus, as observed in the cells transfected with vectors only
208 and treated with poly(I:C) (Fig. 5A and 5B). Little if any VP35 or NP was
209 demonstrated to interact with IRF3 by immunoprecipitation (Fig. 5 – figure
210 supplement 1A-B). Compared to NP/VP35 coexpression, the presence of protein L,
211 VP30 and VP24 showed little, if any, effect on IBs-like structure formation, IRF3
212 sequestration and nuclear IRF3 levels (Fig. 5A and 5B). These results suggested that
213 IBs-like structures as well as VP35 expression were indispensable for IRF3
214 sequestration.

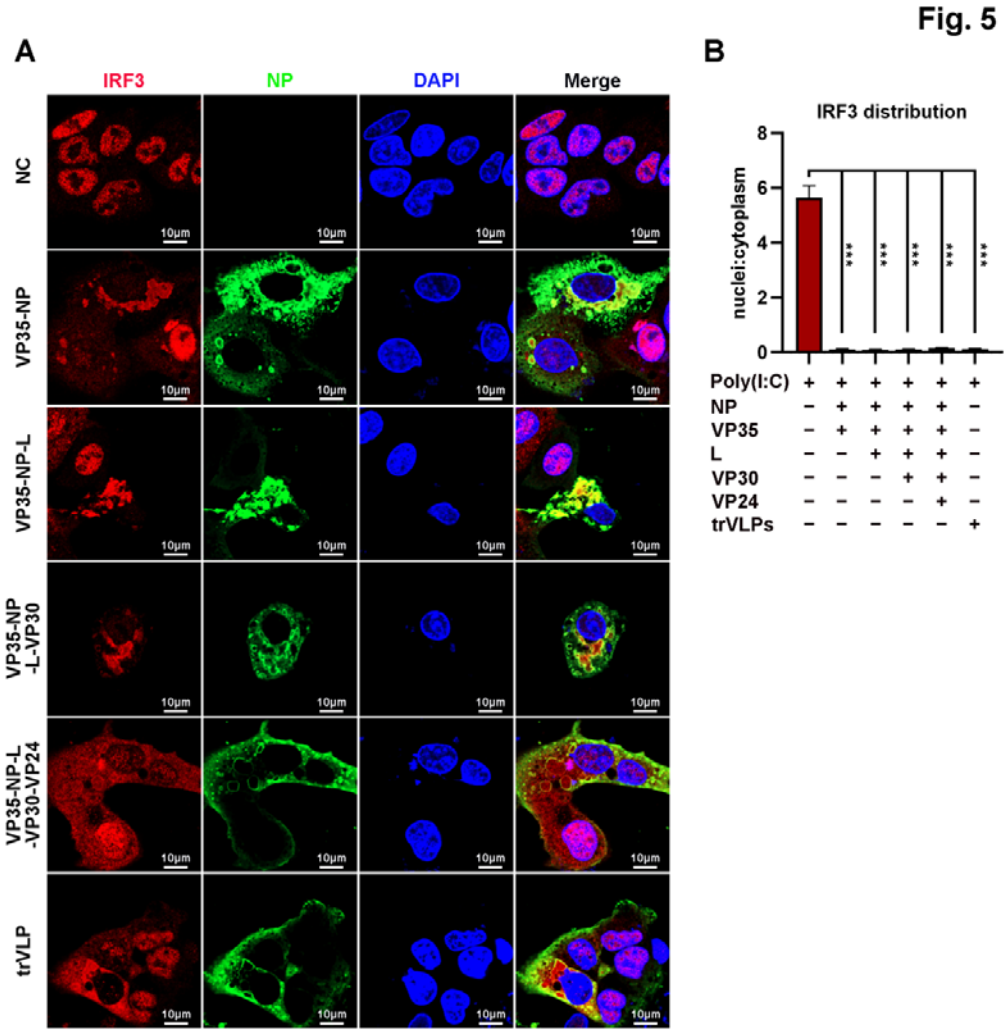

Fig. 5 EBOV NP and VP35 play an important role in sequestering IRF3 into IBs. (A), HepG2 cells were transfected with the indicated plasmids for 36 h, and the cells were treated with 5 μg/ml poly(I:C) for another 12 h. Then, the cells were fixed and immunostained with anti-IRF3 (red) and anti-NP (green) antibodies. Nuclei were stained with DAPI (blue), and images were obtained using a Zeiss LSM 800 Meta confocal microscope. Scale bar, 10 μm. (B), The nuclear/cytoplasmic distribution of IRF3 in (A) was analyzed by ImageJ software. Differences between the two groups were evaluated using a two-sided unpaired Student's *t*-test. The ratio of IRF3 distribution in at least 5 cells from two independent assays is presented as the mean ± SEM (n=5; $^{**}P < 0.01$, $^{***}P$

224 < 0.001).

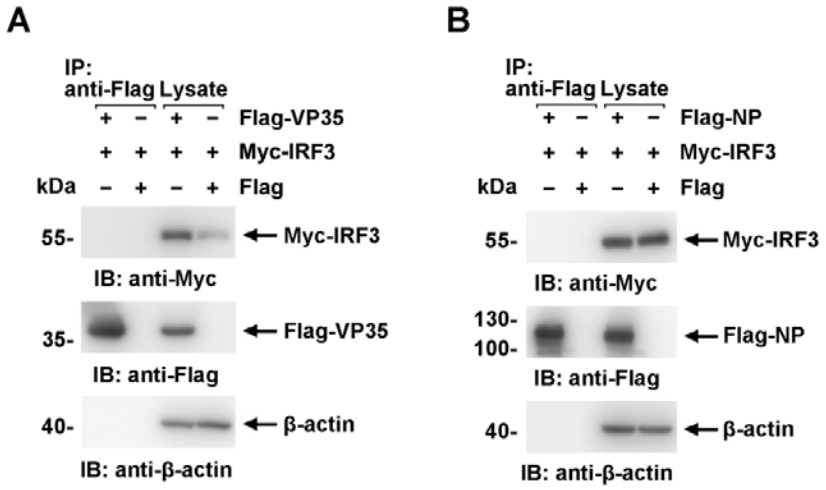

225

226 **Fig. 5 – figure supplement 1. Neither VP35 nor NP interacts directly with IRF3 in cells.** (A
227 and B) Lysates of HEK293 cells transfected with the indicated plasmids were subjected to
228 anti-Flag immunoprecipitation and analyzed by immunoblotting. The data from two independent
229 replicates are presented.

230

231 **VP35: STING interactions play an important role in isolating IRF3 into viral IBs**

232 TBK1 and IKKε were spatially separated from VP35 upon infection by EBOV
233 trVLPs (Fig. 1B and 1C), and IRF3 itself was demonstrated not to interact with VP35
234 (Fig. 5 – figure supplement 1A-B), implying that other IRF3-interacting proteins
235 might be involved in IRF3 sequestration in IBs upon viral infection. Stimulator of IFN
236 genes (STING), an endoplasmic reticulum adaptor associated with IRF3 (Petrasek et
237 al., 2013), was observed to interact with VP35 (Fig. 6A) and be recruited into IBs
238 when the cells were infected by EBOV trVLPs (Fig. 6B and 6C). A substantial portion

239 of STING was found to be recruited into IBs at 36 hpi in EBOV trVLPs-infected cells
240 (Fig. 6D, 6E and Fig. 6 – figure supplement 1). STING knockdown by siRNA
241 inhibited IRF3 sequestration in viral IBs (Fig. 6F and 6G). These results suggested
242 that STING played important roles in the sequestration of IRF3 in viral IBs, possibly
243 by interacting with VP35.

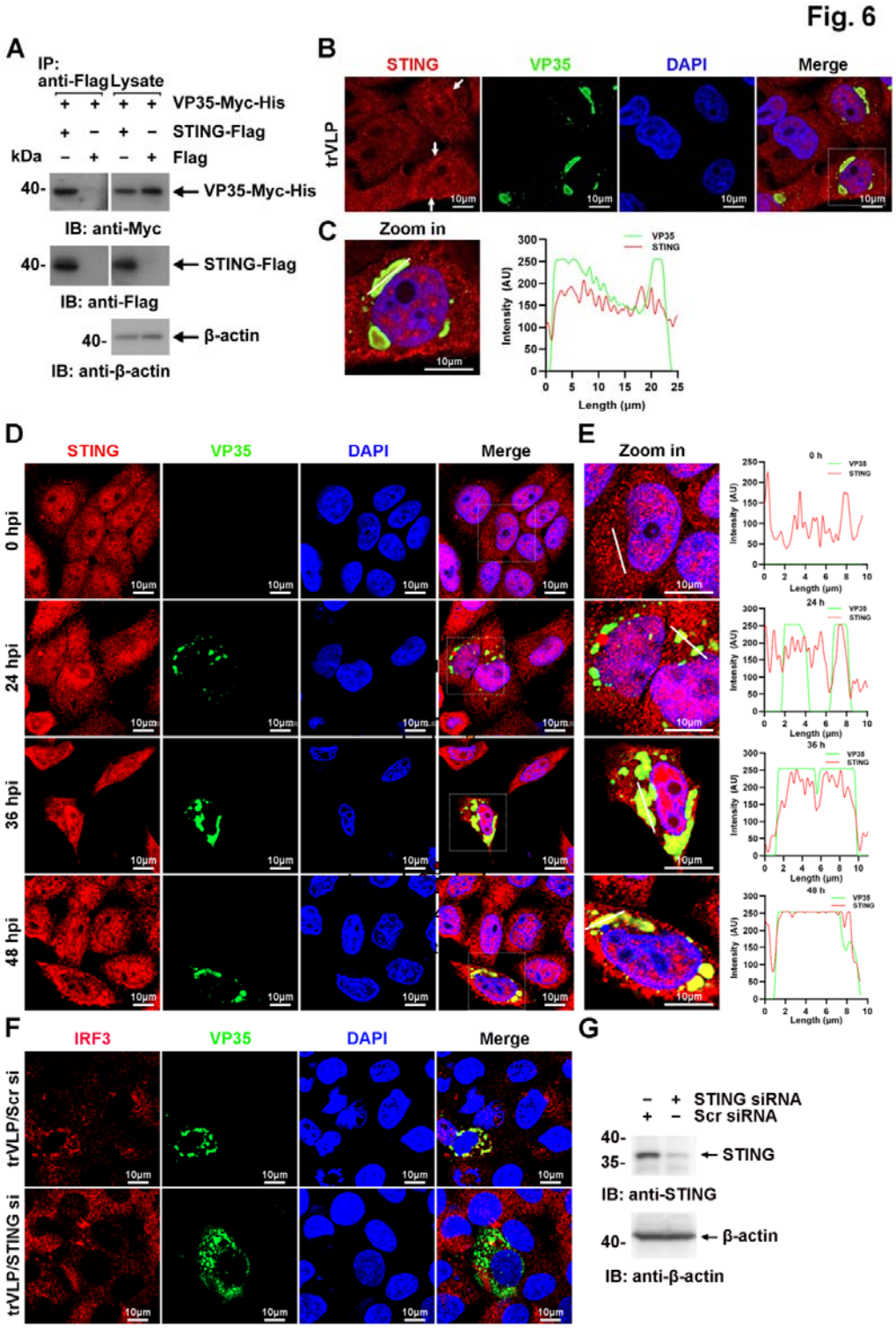

Fig. 6 EBOV trVLP recruit IRF3 into viral IBs via STING. (A), Lysates of HEK293 cells transfected with the indicated plasmids were subjected to anti-Flag immunoprecipitation and

247 analyzed by immunoblotting. (B) HepG2 cells were transfected with the EBOV minigenome (p0).
248 Forty-eight hours after infection, the cells were fixed and immunostained with anti-STING (red)
249 and anti-VP35 (green) antibodies. White arrows: STING in IBs. Nuclei were stained with DAPI
250 (blue), and images were obtained using a Zeiss LSM 800 Meta confocal microscope. Scale bar, 10
251 μm. (C) The left panel shows a magnified image of the IBs boxed in the merged panel of (B). The
252 graphs (right panel) show fluorescent intensity profiles along the indicated white lines drawn
253 across one or more IBs. (D) HepG2 cells were transfected with the EBOV minigenome (p0). At
254 the indicated time points post-transfection, cells were fixed and immunostained with anti-STING
255 (red) and anti-VP35 (green) antibodies. Nuclei were stained with DAPI (blue), and images were
256 obtained using a Zeiss LSM 800 Meta confocal microscope. Scale bar, 10 μm. The data from two
257 independent replicates are presented. (E) The left panel shows a magnified image of the IBs boxed
258 in the merged panel of (D). The graphs (right panel) show fluorescent intensity profiles along the
259 indicated white lines drawn across one or more IBs. (F and G) HepG2 cells were transfected with
260 STING siRNA (STING si) or scrambled siRNA (Scr si) for 6 h. Next, the cells were transfected
261 with the EBOV minigenome (p0) for 36 h and then immunostained with anti-VP35 (green) and
262 anti-IRF3 (red) antibodies. The silencing efficiency of the STING siRNA was determined by
263 immunoblotting (G).

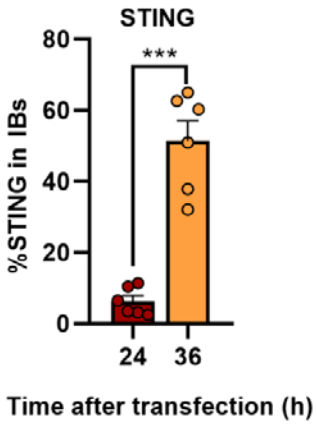

Fig. 6 – figure supplement 1. EBOV trVLP recruit STING into viral IBs. The percentage of STING distribution in IBs at different time points in cells infected with EBOV trVLPs in Fig. 6D was analyzed with R programming language. The intensity of STING in 6 cells from two independent assays is presented as the mean ± SEM (n=6; ***$P < 0.001$).

Viral IBs-induced IRF3 sequestration suppresses IFN-β production

EBOV trVLPs could hijack IRF3 and sequester IRF3 into IBs and thus block the nuclear translocation of IRF3, which suggested that EBOV trVLPs may suppress IRF3-driven IFN-β production. As reported previously (Basler et al., 2000), expression of VP35 (Fig. 7A), but not NP, resulted in a mild inhibition of SeV-induced IFN-β-Luc expression (Fig. 7B). Coexpression of VP35 and NP, which led to the formation of IBs and the sequestration of IRF3 (Fig. 5A), suppressed IFN-β-Luc expression much more potently than VP35 expression alone (Fig. 7B). Coexpression of NP/VP35/L/VP30 was more potent in the inhibition of SeV-induced IFN-β-Luc expression than NP/VP35 (Fig. 7B). Moreover, coexpression of NP/VP35/VP30/L almost completely suppressed poly(I:C)-induced IFN-β transcription (Fig. 7C). *IRF3* depletion showed little, if any, effect on IFN-β

281 transcription upon NP/VP35/L/VP30 coexpression (Fig. 7C), which suggested that
282 NP/VP35/L/VP30 coexpression was similarly powerful as *IRF3* depletion in
283 antagonizing IFN-β expression. These results strongly suggested that viral IBs
284 sequestration of IRF3 was substantially more powerful than that of VP35 expression.

285 We next assessed the effect of IRF3 hijacking and sequestration by viral IBs on
286 EBOV trVLPs replication. Compared with wild-type cells, *IRF3* depletion showed
287 little, if any, effect on EBOV replication, as indicated by luciferase activity,
288 suggesting that trVLPs efficiently blocked IRF3 signaling (Fig. 7D). Moreover,
289 overexpression of IRF3/5D (a phospho-mimic of activated IRF3), but not IRF3,
290 inhibited EBOV trVLPs replication in *IRF3*-depleted cells (Fig. 7D). Taken together,
291 these results suggest that the hijacking of IRF3 and sequestration into IBs by EBOV
292 trVLPs can be significantly more potent in the inhibition of IFN-I production, thereby
293 antagonizing the inhibitory effect of IFN-I on viral replication.

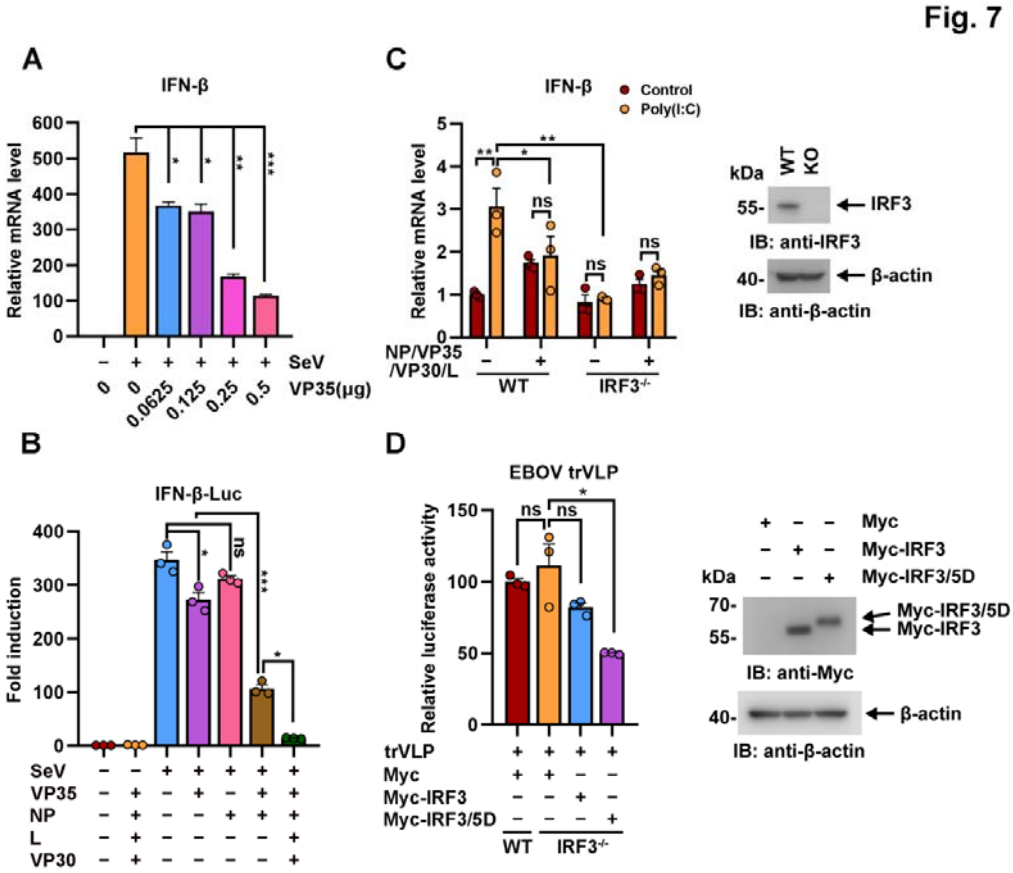

Fig. 7 IRF3 hijacked by viral IBs inhibits IFN-β production. (A), HEK293 cells were transfected with the indicated plasmids for 24 h, and the cells were infected with or without SeV at an MOI of 2 for another 12 h. The mRNA level of IFN-β was quantified using qRT-PCR. Differences between the two groups were evaluated using the two-sided unpaired Student's *t*-test. Data are presented as the mean ± SEM (**P* < 0.05, ***P* < 0.01, ****P* < 0.001). (B), HEK293 cells were cotransfected with the firefly luciferase reporter plasmid pGL3-IFN-β-Luc, the *Renilla* luciferase control plasmid pRL-TK, and viral protein expression plasmids (0.0625 μg pCAGGS-NP, 0.0625 μg pCAGGS-VP35, 0.0375 μg pCAGGS-VP30 and 0.5 μg pCAGGS-L) for 24 h, and the cells were infected with or without SeV at an MOI of 2 for another 12 h. Then, luciferase activities were analyzed. The data were analyzed for fold induction by normalizing the firefly luciferase activity to the *Renilla* luciferase activity. Empty plasmid without SeV infection

306 was used as a control, and the corresponding data point was set to 100%. Differences between the
307 two groups were evaluated using the two-sided unpaired Student's *t*-test. Data are presented as the
308 mean ± SEM (ns, not significant, *$P < 0.05$, ***$P < 0.001$). (C), Wild-type (WT) and
309 *IRF3*-depleted (IRF3$^{-/-}$) HeLa cells were transfected with or without pCASSG-NP, pCASSG-VP35,
310 pCASSG-VP30 and pCASSG-L plasmids for 36 h and then treated with or without 5 μg/ml
311 poly(I:C) for 12 h. The mRNA level of IFN-β was quantified using qRT-PCR (left panel).
312 Differences between the two groups were evaluated using the two-sided unpaired Student's *t*-test.
313 Data are presented as the mean ± SEM (ns, not significant, *$P < 0.05$). Lysates of WT and IRF3$^{-/-}$
314 HeLa cells were analyzed by immunoblotting with an anti-IRF3 antibody (right panel). (D),
315 Wild-type (WT) and *IRF3* knockout (IRF3$^{-/-}$) HeLa cells were transfected with the EBOV
316 minigenome (p0), pGL3-promoter and Myc-vector, Myc-IRF3 or Myc-IRF3/5D plasmids for 96 h.
317 The amounts of trVLPs were determined by luciferase activity assay (left panel). Differences
318 between the two groups were evaluated using the two-sided unpaired Student's *t*-test. Data are
319 presented as the mean ± SEM (ns, not significant, ***$P < 0.001$). Lysates of WT and IRF3$^{-/-}$ HeLa
320 cells transfected with Myc-vector, Myc-IRF3 or Myc-IRF3/5D were analyzed by immunoblotting
321 with the indicated antibodies (right panel).

322

323 **Discussion**

324 Accumulating evidence suggests that EBOV has established multiple ways to
325 antagonize host innate immune responses to maintain viral replication. Several EBOV
326 proteins (VP35, VP24, GP, VP30 and VP40) are known to participate in host immune

327 evasion to facilitate viral replication and pathogenesis (Audet & Kobinger, 2015;
328 Bhattacharyya, 2021; Cantoni & Rossman, 2018). VP35 was demonstrated to
329 suppress IFN-I production by inhibiting IRF3/7 phosphorylation, disrupting DC
330 maturation, and facilitating the escape of immune sensation by dsRNA (Basler, 2015;
331 Cardenas et al., 2006; Messaoudi, Amarasinghe, & Basler, 2015; Prins et al., 2009).
332 VP30 and VP40 suppress RNA silencing by interacting with Dicer and modulating
333 RNA interference components via exosomes, respectively (Fabozzi, Nabel, Dolan, &
334 Sullivan, 2011; Pleet, DeMarino, Lepene, Aman, & Kashanchi, 2017). VP24 and GP
335 are also known to block IFN-I signaling by hiding MHC-1 on the cell surface and
336 counteracting tetherin or interfering with established immune responses by adsorbing
337 antibodies against GP, respectively (Audet & Kobinger, 2015; Bhattacharyya, 2021).

338 Viral IBs are a characteristic of cellular EBOV infection and are important sites
339 for viral RNA replication, and NP and VP35 are extremely critical proteins for the
340 formation of IBs structures (Hoenen et al., 2012). However, whether viral IBs are
341 involved in antagonizing IFN-I production during EBOV trVLPs infection has not yet
342 been reported. Here, we found that IRF3 is hijacked and sequestered into EBOV IBs
343 by viral infection (Fig. 1A), which demonstrates that viral IBs are utilized for IRF3
344 compartmentalization. Meanwhile, this compartmentalization resulted in the spatial
345 isolation of IRF3 from the kinases TBK1 and IKKε (Fig. 1B and 1C). This suggests
346 that IRF3 deprivation by viral IBs may antagonize host antiviral signaling by
347 inhibiting IFN-I production signaling.

348 As expected, the expression of NP/VP35/VP30/L, which is involved in the
349 composition of IBs, was significantly more antagonistic to SeV-induced IFN-β
350 production than the expression of VP35 alone (Fig. 7B). In addition, the expression of
351 NP/VP35/VP30/L can significantly antagonize the promoting effect of poly(I:C) on
352 IFN-β transcription, and IRF3 knockout could not further inhibit the transcription of
353 IFN-β (Fig. 7C), which may be because viral hijacking of IRF3 into IBs nearly
354 completely antagonized its function of promoting IFN-β production. Furthermore,
355 knockout of IRF3 in cells cannot further promote EBOV trVLPs replication compared
356 to wild-type cells (Fig. 7D), which may be because IRF3 is hijacked into viral IBs and
357 cannot be phosphorylated into the nucleus to regulate IFN-I production. These results
358 suggest that viral IBs act as virus-built 'jails' to imprison transcription factors and
359 present a novel and possible common mechanism of viral immune evasion in which
360 the critical signaling molecule IRF3 is spatially segregated from the antiviral kinases
361 TBK1 and IKKε.

362 Although almost all IRF3 could be sequestered to viral IBs formed by VP35 and
363 NP (Fig. 5A and 5B), we found that neither VP35 nor NP interacted with IRF3 (Fig. 5
364 – figure supplement 1). Here, we found that VP35 interacts with STING and
365 colocalizes in IBs and that knockdown of STING inhibits the sequestration of IRF3 in
366 IBs (Fig. 6A-G). These results suggest that VP35 may hijack IRF3 into IBs through
367 STING. However, whether other host proteins are involved in this process and the
368 role of NP in the recruitment of IRF3 by VP35 remains unclear. In addition, we found
369 that VP35 may hijack IRF3 into IBs via STING association (Fig. 6A-6C); however,

370 whether VP35 activates the STING-IRF3 pathway in a cGAS-independent manner by
371 interacting with STING and the molecular mechanism remain to be further
372 investigated.

373 In summary, EBOV VP35 sequesters IRF3 into viral IBs and inhibits the
374 association of IRF3 with TBK1 and IKKε, preventing IRF3 from entering the nucleus
375 and thereby inhibiting IFN-I production (Fig. 8). Therefore, this study reveals a new
376 strategy by which EBOV escapes the innate immune response and provides new ideas
377 for Ebola virus disease treatment.

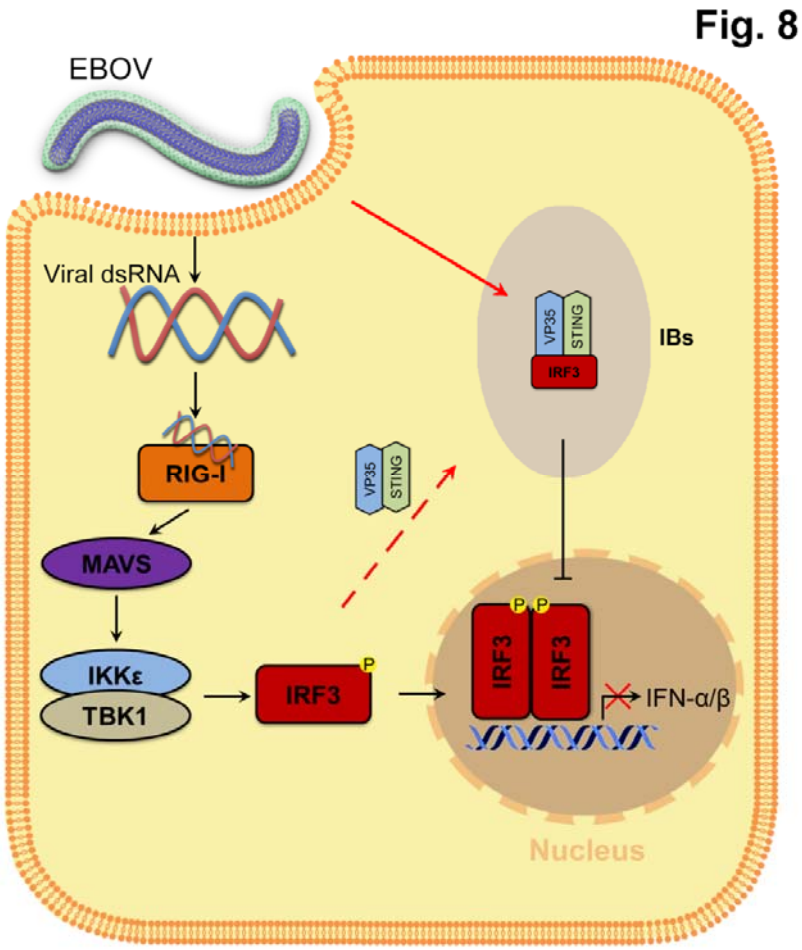

378

379 **Fig. 8 Model of the molecular mechanism by which EBOV hijacks IRF3 into viral IBs**
380 **through VP35-STING to comprehensively disrupt IFN-I production.** VP35 sequesters IRF3 to
381 EBOV IBs, which in turn spatially segregates IRF3 from TBK1 and IKKε , blocks RLR signaling
382 and inhibits IFN-I production.

383

384 # Materials and Methods

385 ## Cell lines and transfections

386 HEK293, HeLa and IRF3-knockout HeLa cells (ABclonal, RM02113) were
387 grown in Dulbecco's modified Eagle's medium (DMEM, Gibco). HepG2 cells were
388 grown in minimum essential medium (MEM, Gibco) supplemented with a 1%
389 nonessential amino acid solution (NEAA, Gibco). All media were supplemented with
390 10% heat-inactivated fetal bovine serum (Gibco), 2 mM L-glutamine, 100 units/ml
391 penicillin and 100 units/ml streptomycin, and cells were grown at 37°C under an
392 atmosphere with 5% CO_2. Transient transfection was performed with Lipofectamine
393 3000 (Invitrogen) according to the manufacturer's instructions.

394 ## Vectors and viruses

395 Flag-tagged VP35, NP, STING, TBK1 and IRF3 vectors were constructed by
396 cloning the corresponding gene fragments into a pcDNA3.0-based Flag-vector
397 (Invitrogen). Myc-tagged VP35, IRF3 and IRF3/5D vectors were constructed by

398 inserting the corresponding gene fragments into the pCMV-Myc vector (Clontech).
399 All the constructs were validated by Sanger DNA sequencing.

400 SeV was amplified in 9- to 11-day embryonated specific pathogen-free (SPF)
401 eggs. Live EBOV (Mayinga strain) is preserved by the BSL-4 Lab at the Wuhan
402 Institute of Virology, Chinese Academy of Sciences.

403 **Immunoprecipitation and immunoblot analysis**

404 Cell lysates were prepared in lysis buffer containing 1% Nonidet P-40 and
405 protease inhibitor cocktail (Roche) (Cao, Leng, & Kufe, 2003). Soluble proteins were
406 immunoprecipitated using anti-Flag (M2, Sigma), anti-Myc (Sigma) or IgG of the
407 same isotype from the same species as a negative control (Sigma). An aliquot of the
408 total lysate (5%, v/v) was included as a control. Immunoblotting was performed with
409 horseradish peroxidase (HRP)-conjugated anti-Myc (Sigma), HRP-conjugated
410 anti-Flag (Sigma), HRP-conjugated anti-β-actin (Sigma), anti-VP35 (Creative
411 Diagnostics), anti-IRF3 (Cell Signaling Technology), anti-STING (Proteintech) or
412 anti-NP (Sino Biological) antibodies. The antigen-antibody complexes were
413 visualized via chemiluminescence (Immobilon Western Chemiluminescent HRP
414 Substrate, Millipore). A PageRuler Western marker (Thermo) was used as a molecular
415 weight standard.

416 **Gene silencing using siRNA**

417 For gene knockdown in HepG2 cells, cells maintained in 6-well plates were
418 transfected with 100 pmol STING small interfering RNA (siRNA) (sense, 5'-
419 GCACCUGUGUCCUGGAGUATT -3'; antisense, 5'-
420 UACUCCAGGACACAGGUGCTT -3') or the same concentration of scrambled
421 siRNA (sense, 5'- UUCUCCGAACGUGUCACGUTT -3'; antisense, 5'-
422 ACGUGACACGUUCGGAGAATT -3') purchased from Tsingke Biotechnology
423 (Beijing, China) with Lipofectamine 3000 (Invitrogen) according to the
424 manufacturer's recommendations.

425 **Reverse transcription and quantitative RT-PCR**

426 Total cellular RNA was prepared using an RNeasy Mini kit (QIAgen, USA)
427 according to the manufacturer's protocol. For cDNA synthesis, 0.5 μg of RNA was
428 first digested with gDNA Eraser to remove contaminated DNA and then reverse
429 transcribed using ReverTra Ace qPCR RT Master Mix with gDNA Remover
430 (FSQ-301, Toyobo) in a 20 μL reaction volume. Then, 1 μL of cDNA was used as a
431 template for quantitative PCR. The following primers were used in these experiments:
432 h-IFN-β F: 5'-AGGACAGGATGAACTTTGAC-3'
433 h-IFN-β R: 5'-TGATAGACATTAGCCAGGAG-3'
434 h-GAPDH F: 5'-AAggTCATCCCTgAgCTgAAC-3'
435 h-GAPDH R: 5'-ACgCCTgCTTCACCACCTTCT-3'

436 The samples were denatured at 95°C for 2 min, followed by 40 cycles of
437 amplification (15 s at 94°C for denaturation, 60 s at 60°C for annealing and extension).

Quantitative RT-PCR (qRT-PCR) was performed using SYBR Green Real-time PCR Master Mix (QPK-201, Toyobo) with the QuantStudio 6 Flex multicolor real-time PCR detection system (ABI). Relative mRNA levels were normalized to GAPDH levels and calculated using the $2^{-\Delta\Delta CT}$ method (Livak & Schmittgen, 2001). The means (upper limit of the box) ± SEM (error bars) of three independent experiments are presented in the figures.

In situ proximity ligation assay

Duolink *in situ* PLA (Sigma) was used to detect the endogenous association of IRF3 and TBK1 in cells. In brief, HepG2 cells plated on glass coverslips were transfected with EBOV minigenome plasmids. After fixation with 4% formaldehyde, the cells were permeabilized with 0.3% Triton X-100 in PBS for 15 min. After blocking with blocking buffer (Sigma, DUO82007), the cells were incubated with mouse anti-IRF3 (Cell Signaling Technology) and rabbit anti-TBK1 (Abcam) primary antibodies. The nuclei were stained with DAPI (blue). The red fluorescent spots generated from the DNA amplification-based reporter system combined with oligonucleotide-labeled secondary antibodies were detected with a Zeiss LSM 800 Meta confocal microscope (Carl Zeiss).

Immunofluorescence microscopy

Cells were transfected, fixed, permeabilized and blocked as described above. Then, after incubation with anti-TBK1 (Cell Signaling Technology), anti-IKKε (Cell

458 Signaling Technology), anti-IRF3 (Cell Signaling Technology), anti-VP35 (Creative
459 Diagnostics), anti-NP (Sino Biological) or anti-STING (Bioss) antibodies overnight at
460 4°C, the cells were washed three times with blocking solution and then incubated with
461 FITC- or TRITC-conjugated goat anti-rabbit (or anti-mouse) IgG. The cells were then
462 stained with DAPI after washing and imaged using a laser scanning confocal
463 microscope (Zeiss LSM 800 Meta) with a 63× oil immersion lens.

464 **Luciferase reporter assay**

465 The IFN-I production assay was performed as described previously (Zhu et al.,
466 2022). Briefly, HEK293 cells (1×10^5 cells per well in a 24-well plate) were
467 cotransfected with the indicated amount of pCAGGS-NP (75 ng)/pCAGGS-VP35 (75
468 ng)/pCAGGS-VP30 (37.5 ng)/pCAGGS-L (500 ng), 200 ng of the IFN-β reporter
469 plasmid (Promega, USA) and 4 ng of *Renilla* luciferase plasmid. An empty vector was
470 used to ensure that each well contained the same plasmid concentration. After 24 h,
471 the cells were treated with SeV (MOI=2) or 5 μg/ml poly(I:C) for 12 h, and the
472 luciferase activity of the cell lysates was analyzed with the dual-luciferase reporter
473 assay system (Promega, E1960) using a GloMax 20/20 luminometer (Promega, USA).
474 Values were obtained by normalizing the luciferase values to the Renilla values. Fold
475 induction was determined by setting the results from the group transfected with vector
476 without Flag-VP35 to a value of 1.

477 **EBOV trVLPs assay**

478 The replication of EBOV in the cells was evaluated with the minigenome system
479 (Hoenen et al., 2014). Briefly, producer cells (p0) were cotransfected with
480 p4cis-vRNA-RLuc (250 ng) and pCAGGS-T7 (250 ng) for T7 RNA polymerase
481 expression and 4 plasmids for EBOV protein expression (pCAGGS-NP (125 ng),
482 pCAGGS-VP35 (125 ng), pCAGGS-VP30 (75 ng), and pCAGGS-L (1,000 ng)), as
483 well as the luciferase reporter vector pGL3-Promoter (Youbio, 25 ng). One day after
484 transfection, the medium was replaced with medium containing 5% FBS, and the cells
485 were then incubated for another 3 days. Viral replication was determined by
486 intracellular luciferase activities using a dual-luciferase reporter assay kit (Promega,
487 E1960) after cell lysis with passive lysis buffer (PLB, Promega). For
488 immunofluorescence experiments, cells were harvested 48 h after transfection.

489 **Transmission electron microscopy (TEM)**

490 HepG2 cells transfected with EBOV minigenome p0-related plasmids were
491 washed with PBS, fixed with 2.5% glutaraldehyde, and then prestained with osmium
492 tetroxide. Eighty-nanometer-thick serial sections were then cut and stained with
493 uranyl acetate and lead citrate. Images were acquired with a transmission electron
494 microscope (Hitachi, H-7650) operating at 80 kV.

495 **EBOV infection assay**

496 WT HepG2 cells grown in 12-well plates were incubated with the EBOV
497 Mayinga strain at an MOI of 10 as determined by virus titration in Vero E6 cells at

498 37°C for 1 h for microscopy. Then, the cells were washed 3 times with PBS, and fresh
499 medium was added to the cells, which were incubated at 37°C for 72 h. Subsequently,
500 the cells were fixed with 4% formaldehyde for immunofluorescence microscopy as
501 required by the BSL-4 laboratory. All work with live EBOV was performed with
502 BSL-4 containment.

503 **Statistical analyses**

504 Graphical representation and statistical analyses were performed using Prism 8
505 software (GraphPad Software). Unless indicated otherwise, the results are presented
506 as the means (upper limit of the box) ± SEM (error bars) from three independent
507 experiments conducted in duplicate. An unpaired two-tailed *t*-test was used for the
508 analysis of two groups. Data were considered significant when $P < 0.05$ (*), $P < 0.01$
509 (**), and $P < 0.001$ (***).

510

511 **Data availability**

512 All the data shown in this paper are available from the corresponding authors upon
513 reasonable request.

514 **Acknowledgments**

515 This work was supported by the Advanced Customer Cultivation Project of Wuhan
516 National Biosafety Laboratory, Chinese Academy of Sciences [2022ACCP-MS04]

and the National Major Science and Technology Projects of China [2018ZX09711003-005-005 to T.G., 2022YFC2600704 to H.L.].

Competing Interests statement

The authors declare no competing interests.

Author Contributions

L.Z., X.L., and C.C. designed and supervised the study. L.Z., J.J., and T.W. performed the experiments. T.G., H.L., Q.D., Y.H., Y. J., Z.L, and P. L. analyzed the data. L.Z, X.L., and C.C. wrote the manuscript. All authors have read and approved the article.

References

Audet, J., & Kobinger, G. P. (2015). Immune evasion in ebolavirus infections. *Viral Immunol, 28*(1), 10-18. doi: 10.1089/vim.2014.0066

Basler, C. F. (2015). Innate immune evasion by filoviruses. *Virology, 479-480*, 122-130. doi: 10.1016/j.virol.2015.03.030

Basler, C. F., Mikulasova, A., Martinez-Sobrido, L., Paragas, J., Muhlberger, E., Bray, M., Klenk, H. D., Palese, P., & Garcia-Sastre, A. (2003). The Ebola Virus VP35 Protein Inhibits Activation of Interferon Regulatory Factor 3. *J Virol, 77*(14), 7945-7956. doi: 10.1128/jvi.77.14.7945-7956.2003

Basler, C. F., Wang, X., Muhlberger, E., Volchkov, V., Paragas, J., Klenk, H. D., Garcia-Sastre, A., & Palese, P. (2000). The Ebola virus VP35 protein functions as a type I IFN antagonist. *P Natl Acad Sci Usa, 97*(22), 12289-12294. doi: 10.1073/pnas.220398297

Bhattacharyya, S. (2021). Mechanisms of Immune Evasion by Ebola Virus. *Adv Exp Med Biol, 1313*, 15-22. doi: 10.1007/978-3-030-67452-6_2

Cantoni, D., & Rossman, J. S. (2018). Ebolaviruses: New roles for old proteins. *PLoS Negl Trop Dis, 12*(5), e0006349. doi: 10.1371/journal.pntd.0006349

Cao, C., Leng, Y., & Kufe, D. (2003). Catalase activity is regulated by c-Abl and Arg in the oxidative stress response. *J Biol Chem, 278*(32), 29667-29675. doi: 10.1074/jbc.M301292200

Cardenas, W. B., Loo, Y. M., Gale, M., Jr., Hartman, A. L., Kimberlin, C. R., Martinez-Sobrido, L., Saphire, E. O., & Basler, C. F. (2006). Ebola virus VP35 protein binds double-stranded RNA and inhibits alpha/beta interferon production induced by RIG-I signaling. *J Virol, 80*(11), 5168-5178. doi: 10.1128/JVI.02199-05

Fabozzi, G., Nabel, C. S., Dolan, M. A., & Sullivan, N. J. (2011). Ebolavirus proteins suppress the

effects of small interfering RNA by direct interaction with the mammalian RNA interference pathway. *J Virol, 85*(6), 2512-2523. doi: 10.1128/JVI.01160-10

Feldmann, H., Jones, S., Klenk, H. D., & Schnittler, H. J. (2003). Ebola virus: from discovery to vaccine. *Nat Rev Immunol, 3*(8), 677-685.

Fitzgerald, K. A., McWhirter, S. M., Faia, K. L., Rowe, D. C., Latz, E., Golenbock, D. T., Coyle, A. J., Liao, S. M., & Maniatis, T. (2003). IKKepsilon and TBK1 are essential components of the IRF3 signaling pathway. *Nat Immunol, 4*(5), 491-496. doi: 10.1038/ni921

Haasnoot, J., de Vries, W., Geutjes, E. J., Prins, M., de Haan, P., & Berkhout, B. (2007). The Ebola virus VP35 protein is a suppressor of RNA silencing. *Plos Pathog, 3*(6), 794-803. doi: 10.1371/journal.ppat.0030086

Hoenen, T., Shabman, R. S., Groseth, A., Herwig, A., Weber, M., Schudt, G., Dolnik, O., Basler, C. F., Becker, S., & Feldmann, H. (2012). Inclusion Bodies Are a Site of Ebolavirus Replication. *J Virol, 86*(21), 11779-11788. doi: 10.1128/jvi.01525-12

Hoenen, T., Watt, A., Mora, A., & Feldmann, H. (2014). Modeling the lifecycle of Ebola virus under biosafety level 2 conditions with virus-like particles containing tetracistronic minigenomes. *Jove-J Vis Exp, 91*(l), e52381. doi: 10.3791/52381

Hong, Y., Bai, M., Qi, X., Li, C., Liang, M., Li, D., Cardona, C. J., & Xing, Z. (2019). Suppression of the IFN-alpha and -beta Induction through Sequestering IRF7 into Viral Inclusion Bodies by Nonstructural Protein NSs in Severe Fever with Thrombocytopenia Syndrome Bunyavirus Infection. *J Immunol, 202*(3), 841-856. doi: 10.4049/jimmunol.1800576

Lee, J. K., & Shin, O. S. (2021). Nonstructural Protein of Severe Fever with Thrombocytopenia Syndrome Phlebovirus Inhibits TBK1 to Evade Interferon-Mediated Response. *J Microbiol Biotechnol, 31*(2), 226-232. doi: 10.4014/jmb.2008.08048

Liu, S., Cai, X., Wu, J., Cong, Q., Chen, X., Li, T., Du, F., Ren, J., Wu, Y. T., Grishin, N. V., & Chen, Z. J. (2015). Phosphorylation of innate immune adaptor proteins MAVS, STING, and TRIF induces IRF3 activation. *Science, 347*(6227), aaa2630. doi: 10.1126/science.aaa2630

Livak, K. J., & Schmittgen, T. D. (2001). Analysis of relative gene expression data using real-time quantitative PCR and the 2(-Delta Delta C(T)) Method. *Methods, 25*(4), 402-408. doi: 10.1006/meth.2001.1262

Mahanty, Siddhartha, & Bray, Mike. (2004). Pathogenesis of filoviral haemorrhagic fevers. *Lancet Infect Dis, 4*(8), 487-498. doi: 10.1016/s1473-3099(04)01103-x

McCarthy, S. D., Majchrzak-Kita, B., Racine, T., Kozlowski, H. N., Baker, D. P., Hoenen, T., Kobinger, G. P., Fish, E. N., & Branch, D. R. (2016). A Rapid Screening Assay Identifies Monotherapy with Interferon-ss and Combination Therapies with Nucleoside Analogs as Effective Inhibitors of Ebola Virus. *PLoS Negl Trop Dis, 10*(1), e0004364. doi: 10.1371/journal.pntd.0004364

Messaoudi, Ilhem, Amarasinghe, Gaya K., & Basler, Christopher F. (2015). Filovirus pathogenesis and immune evasion: insights from Ebola virus and Marburg virus. *Nat Rev Microbiol, 13*(11), 663-676. doi: 10.1038/nrmicro3524

Misasi, J., & Sullivan, N. J. (2014). Camouflage and misdirection: the full-on assault of Ebola virus disease. *Cell, 159*(3), 477-486. doi: 10.1016/j.cell.2014.10.006

Nanbo, Asuka, Watanabe, Shinji, Halfmann, Peter, & Kawaoka, Yoshihiro. (2013). The spatio-temporal distribution dynamics of Ebola virus proteins and RNA in infected cells. *Sci Rep, 3*(1), 1206. doi: 10.1038/srep01206

Ning, Y. J., Feng, K., Min, Y. Q., Cao, W. C., Wang, M., Deng, F., Hu, Z., & Wang, H. (2015).

Disruption of type I interferon signaling by the nonstructural protein of severe fever with thrombocytopenia syndrome virus via the hijacking of STAT2 and STAT1 into inclusion bodies. *J Virol, 89*(8), 4227-4236. doi: 10.1128/JVI.00154-15

Ning, Y. J., Wang, M., Deng, M., Shen, S., Liu, W., Cao, W. C., Deng, F., Wang, Y. Y., Hu, Z., & Wang, H. (2014). Viral suppression of innate immunity via spatial isolation of TBK1/IKKepsilon from mitochondrial antiviral platform. *J Mol Cell Biol, 6*(4), 324-337. doi: 10.1093/jmcb/mju015

Noda, T., Kolesnikova, L., Becker, S., & Kawaoka, Y. (2011). The importance of the NP: VP35 ratio in Ebola virus nucleocapsid formation. *J Infect Dis, 204 Suppl 3*, S878-883. doi: 10.1093/infdis/jir310

Noda, T., Watanabe, S., Sagara, H., & Kawaoka, Y. (2007). Mapping of the VP40-binding regions of the nucleoprotein of Ebola virus. *J Virol, 81*(7), 3554-3562. doi: 10.1128/JVI.02183-06

Petrasek, J., Iracheta-Vellve, A., Csak, T., Satishchandran, A., Kodys, K., Kurt-Jones, E. A., Fitzgerald, K. A., & Szabo, G. (2013). STING-IRF3 pathway links endoplasmic reticulum stress with hepatocyte apoptosis in early alcoholic liver disease. *P Natl Acad Sci Usa, 110*(41), 16544-16549. doi: 10.1073/pnas.1308331110

Pleet, M. L., DeMarino, C., Lepene, B., Aman, M. J., & Kashanchi, F. (2017). The Role of Exosomal VP40 in Ebola Virus Disease. *DNA Cell Biol, 36*(4), 243-248. doi: 10.1089/dna.2017.3639

Prins, K. C., Cardenas, W. B., & Basler, C. F. (2009). Ebola virus protein VP35 impairs the function of interferon regulatory factor-activating kinases IKKε and TBK-1. *J Virol, 83*(7), 3069-3077. doi: 10.1128/JVI.01875-08

Reid, S. P., Cardenas, W. B., & Basler, C. F. (2005). Homo-oligomerization facilitates the interferon-antagonist activity of the ebolavirus VP35 protein. *Virology, 341*(2), 179-189. doi: 10.1016/j.virol.2005.06.044

Reid, S. P., Leung, L. W., Hartman, A. L., Martinez, O., Shaw, M. L., Carbonnelle, C., Volchkov, V. E., Nichol, S. T., & Basler, C. F. (2006). Ebola virus VP24 binds karyopherin alpha1 and blocks STAT1 nuclear accumulation. *J Virol, 80*(11), 5156-5167. doi: 10.1128/JVI.02349-05

van Tol, S., Kalveram, B., Ilinykh, P. A., Ronk, A., Huang, K., Aguilera-Aguirre, L., Bharaj, P., Hage, A., Atkins, C., Giraldo, M. I., Wakamiya, M., Gonzalez-Orozco, M., Warren, A. N., Bukreyev, A., Freiberg, A. N., & Rajsbaum, R. (2022). Ubiquitination of Ebola virus VP35 at lysine 309 regulates viral transcription and assembly. *PLoS Pathog, 18*(5), e1010532. doi: 10.1371/journal.ppat.1010532

Wu, X., Qi, X., Qu, B., Zhang, Z., Liang, M., Li, C., Cardona, C. J., Li, D., & Xing, Z. (2014). Evasion of antiviral immunity through sequestering of TBK1/IKKepsilon/IRF3 into viral inclusion bodies. *J Virol, 88*(6), 3067-3076. doi: 10.1128/JVI.03510-13

Yen, B., Mulder, L. C., Martinez, O., & Basler, C. F. (2014). Molecular basis for Ebolavirus VP35 suppression of human dendritic cell maturation. *J Virol, 88*(21), 12500-12510. doi: 10.1128/JVI.02163-14

Zhu, Lin, Gao, Ting, Huang, Yi, Jin, Jing, Wang, Di, Zhang, Leike, Jin, Yanwen, Li, Ping, Hu, Yong, Wu, Yan, Liu, Hainan, Dong, Qincai, Wang, Guangfei, Zheng, Tong, Song, Caiwei, Bai, Yu, Zhang, Xun, Liu, Yaoning, Yang, Weihong, Xu, Ke, Zou, Gang, Zhao, Lei, Cao, Ruiyuan, Zhong, Wu, Xia, Xianzhu, Xiao, Gengfu, Liu, Xuan, & Cao, Cheng. (2022). Ebola virus VP35 hijacks the PKA-CREB1 pathway for replication and pathogenesis by AKIP1 association. *Nat Commun, 13*(1). doi: 10.1038/s41467-022-29948-4

Zhu, Lin, Gao, Ting, Yang, Weihong, Liu, Yaoning, Liu, Xuan, Hu, Yong, Jin, Yanwen, Li, Ping, Xu,

Ke, Zou, Gang, Zhao, Lei, Cao, Ruiyuan, Zhong, Wu, Xia, Xianzhu, & Cao, Cheng. (2020). Ebola virus replication is regulated by the phosphorylation of viral protein VP35. *Biochem Bioph Res Co, 521*(3), 687-692. doi: 10.1016/j.bbrc.2019.10.147